

Universal momentum distributions for the spin-singlet NN channels*

O. A. Rubtsova[†] V. N. Pomerantsev[‡] L. D. Blokhintsev[§]

Skobeltsyn Institute of Nuclear Physics, Lomonosov Moscow State University, 119991 Moscow, Russia

Abstract: The formalism for a quantitative treatment of high-momentum components of NN momentum distributions for the spin-singlet channels is presented. This approach suggests that the use of a distribution for a virtual state in momentum representation for the NN channel in question is a universal one, which can be further employed within contact formalisms for nuclei. It is shown how such distributions can be calculated from low-energy scattering wave functions in the same channels. As a result, a new characteristic (a constant) for the high-momentum part of the momentum distribution in a spin-singlet channel is introduced. To test the approach, we calculate the pp nuclear contacts for the ^3He , nucleus which appear to be nearly the same for four realistic NN interactions with essentially different high-momentum properties. The results should be useful for researchers studying the problem of short-range correlations in nuclei. In particular, the approach gives a generalization for the formalisms based on nuclear contacts.

Keywords: short-range correlations, momentum distributions, nucleon-nucleon interaction, light nuclei

DOI: 10.1088/1674-1137/addaaf **CSTR:** 32044.14.ChinesePhysicsC.49104104

I. INTRODUCTION

The problem of short-range correlations (SRC) is very relevant nowadays due to recent theoretical and experimental achievements [1–8]. The new experiments allow us to count correlated nucleon pairs with high relative momentum and small center of mass momentum. The theoretical description of the corresponding cross-sections in quasi-elastic kinematics is reduced, in many cases, to treatment of the momentum distributions of nucleons in nuclei. This gives rise to the contact formalisms [9, 10], which appear to be convenient for practical calculations [5].

In this paper, we discuss one of the key aspects of the SRC problem. The two-nucleon momentum distribution ρ_{NN}^A in the nucleus A depends on the relative momentum of nucleons k , the momentum of their center of mass Q , and the angle θ between the corresponding vectors. These distributions have similar properties for different nuclei [11] and satisfy the factorization property at high relative momenta k and low Q [9, 12]:

$$\rho_{NN}^A(k, Q, \theta) \approx C_{NN}^A \rho_{NN}(k) \rho_{\text{cm}}^{A, NN}(Q), \quad (1)$$

where C_{NN}^A is a constant depending on the nucleus A (the

so-called nuclear contact), $\rho_{\text{cm}}^{A, NN}(Q)$ is a distribution of center-of-mass momentum for a pair of nucleons in the nucleus, while $\rho_{NN}(k)$ represents a universal two-nucleon momentum distribution (UMD) that does not depend on A [9]. The high-momentum part of this distribution depends on the chosen model of NN interaction. In the case of spin-triplet np pairs, this universal distribution coincides with the distribution of nucleons in the deuteron: $\rho_{np}(k) = \rho_d(k)$. Because $\rho_d(k)$ is normalized to 1, one can explicitly calculate a weight of the high-momentum part of the distribution a_2^d [13], which determines the magnitude of SRC.

At the same time, for spin-singlet 1S_0 NN channels (*i.e.*, np , pp , and nn), bound states are absent and there is a problem of determining the corresponding universal distributions [9], as well as estimating the magnitude of high-momentum components for such states for two-nucleon system. In [12], the corresponding momentum distributions at $Q = 0$ in ^4He were considered as universal distributions for pp (or nn) pairs, and factorization (1) was used to calculate spectral functions for heavier nuclei up to ^{40}Ca . Another approach to determining the UMD for spin-singlet pairs was proposed within the Generalized Contact Formalism (GCF) [5, 10] by using the two-body NN scattering wave functions at zero energy, which are normalized by their high-momentum tails, *i.e.*, the integ-

Received 10 April 2025; Accepted 20 May 2025; Published online 21 May 2025

* The study was conducted under the state assignment of Lomonosov Moscow State University

[†] E-mail: rubtsova@nucl-th.sinp.msu.ru

[‡] E-mail: pomeran@nucl-th.sinp.msu.ru

[§] E-mail: blokh@srd.sinp.msu.ru

©2025 Chinese Physical Society and the Institute of High Energy Physics of the Chinese Academy of Sciences and the Institute of Modern Physics of the Chinese Academy of Sciences and IOP Publishing Ltd. All rights, including for text and data mining, AI training, and similar technologies, are reserved.

ral from some p_0 (the boundary of the high-momentum region) to infinity. However, the problem of quantitatively evaluating the high-momentum components for spin-singlet channels, which would allow comparison of different NN interactions in this regard, still remains open.

In the present paper, we propose a universal distribution for singlet NN channels that does not depend on the boundary of the high-momentum region p_0 and is determined directly by the momentum distribution for the virtual state. It should be noted that such a distribution for a particular case of a separable NN interaction was used as a two-body pp -distribution in Ref. [14]. In a general case, to obtain the momentum distribution for virtual state, one can use the low-energy scattering wave functions.

For this purpose, we use the approach of Fäldt and Wilkin [15, 16], which established a relation between the scattering and bound state wave functions and was applied to inelastic NN scattering calculations [17]. This approach gives an explicit factor (the Fäldt-Wilkin factor) that allows the bound- and virtual-state momentum distributions to be approximately reproduced in the high-momentum region by using the low-energy scattering wave functions. As a result of the developed technique, we introduce high-momentum constants for different NN interactions in the spin-singlet channel and compare quantitatively high-momentum parts of momentum distributions for different models of NN interactions. Our recently suggested treatment [18] for high-momentum components of the scattering wave functions is helpful for this.

As a numerical illustration, we calculate the nuclear contacts for pp momentum distributions in ^3He with respect to the introduced two-nucleon momentum distributions for four realistic but essentially different models of NN and $3N$ interaction and show that these contacts have nearly the same values. Thus, the suggested formalism can be considered as an extension of the formalism presented in Ref. [9] for np triplet momentum distributions.

The paper is organized as follows. In Sec. II, we derive a relation between the scattering and bound- or virtual-state wave functions and define an explicit factor, *i.e.*, the Fäldt-Wilkin factor. In Sec. III, the found relations are tested for the separable interaction when the virtual-state momentum distribution is found analytically and for the realistic NN interaction as well. In Sec. IV, the UMDs for the spin-singlet NN channels are introduced based on the developed formalism, and the values of the high-momentum constants a_2^v are presented for four different models of NN interaction. In Sec. V, the nuclear contacts for the ^3He nucleus are calculated based on the two-nucleon UMDs. A summary is given in Sec. VI. For the reader's convenience, a small Appendix A gives the explicit relations between different universal momentum distribu-

tions.

II. MOMENTUM DISTRIBUTIONS FOR A TWO-NUCLEON SYSTEM

A. Bound-state, virtual-state, and scattering wave functions

Let's start with the definitions which we will use below.

For the spin-triplet bound state, the two-nucleon momentum distribution is naturally introduced by using the deuteron wave function with the S -wave and D -wave components $u(k)$ and $w(k)$, respectively:

$$\rho_d(k) = |u(k)|^2 + |w(k)|^2, \quad \int_0^\infty dk k^2 \rho_d(k) = 1. \quad (2)$$

The S -matrix $S(p)$ for the spin-triplet np -scattering (here, $p = \sqrt{2\mu E}/\hbar$ is the on-shell momentum) has a pole in a complex p -plane at $p = i\kappa_d$, where $\kappa_d \equiv \sqrt{-2\mu E_d/\hbar^2} > 0$ is the wave number corresponding to the bound-state energy E_d , and μ is the reduced mass of two nucleons.

The corresponding residues of the S -matrix elements at this pole determine the asymptotic normalization coefficients (ANCs) N_S and N_D (see Sec. II.D), which set amplitudes of components of the deuteron wave function in configuration space at $r \rightarrow \infty$:

$$u(r) \rightarrow N_S \exp(-\kappa_d r), \quad w(r) \rightarrow N_D \exp(-\kappa_d r), \quad r \rightarrow \infty \quad (3)$$

provided that the deuteron wave function is normalized to unity: $\int_0^\infty [u^2(r) + w^2(r)] dr = 1$.

There are no bound NN states in the spin-singlet channel 1S_0 . However, in this channel, there is a virtual state $u_v(r)$ with $E_v < 0$ (for the np system $E_v \approx -67$ keV). The pole of the S -matrix corresponding to the virtual state lies on the unphysical energy sheet and on the negative imaginary semi-axis in the complex p -plane at $p = i\kappa_v$:

$$\kappa_v \equiv -\sqrt{-2\mu E_v/\hbar^2}, \quad \kappa_v < 0. \quad (4)$$

The function $u_v(r)$ grows exponentially at the asymptotics:

$$u_v(r) \rightarrow N_v \exp(|\kappa_v| r), \quad r \rightarrow \infty, \quad (5)$$

in contrast to the bound-state case. However, the constant N_v in Eq. (5) is the ANC for a virtual state, which is related to the residue of the S -matrix $S(p)$ for the singlet state at the pole $p = i\kappa_v$.

It should be noted that although the virtual state func-

tion in the coordinate representation $u_v(r)$ with the asymptotics (5) cannot be normalized, the virtual state wave function in the momentum representation $u_v(k)$ is square integrable [19] (also see the example with a separable potential in Sec. III). One can also define a special Fourier transform procedure that relates the coordinate and momentum representations for the virtual-state wave function [20].

Therefore, one can consider the momentum distribution for the virtual state in a similar manner as for the bound-state (2) as follows:

$$\rho_v(k) = |u_v(k)|^2. \quad (6)$$

This distribution has the same dimension as for the bound-state, however, it is not normalized to unity. It would be convenient to define the UMD for the spin-singlet NN channels based on these distributions for virtual states. However, a practical calculation of such a momentum distribution could be complicated for realistic NN interactions. Thus, we will show how to reconstruct it in the high-momentum region just from the low-energy scattering wave functions for the same interaction.

Finally, we introduce the scattering wave functions here. Below, we consider the radial parts of the scattering wave functions ψ_p^s and $\psi_{p,l=0,2}^t$ for two main NN configurations 1S_0 and 3S_1 - 3D_1 both in coordinate and momentum representations. In the momentum space, these functions are normalized as follows:

$$\begin{aligned} \int_0^\infty dk k^2 \psi_p^s(k) \psi_{p'}^s(k) &= \frac{\delta(p-p')}{p^2}, \\ \sum_{l=0,2} \int_0^\infty dk k^2 \psi_{p,l}^t(k) \psi_{p',l}^t(k) &= \frac{\delta(p-p')}{p^2}, \end{aligned} \quad (7)$$

where p is the on-shell momentum.

In the configuration space, we consider functions that satisfy the asymptotic condition of a standing wave. For a singlet channel, this means

$$\psi_p^s(r) \rightarrow \sqrt{\frac{2}{\pi}} \frac{\sin(pr + \phi(p))}{p}, \quad r \rightarrow \infty, \quad (8)$$

where $\phi(p)$ is the partial phase shift.

B. Relation between scattering and bound or virtual state wave functions

In Ref. [15], the authors found an explicit relation between bound-state and scattering wave functions for the same Hamiltonian in case of the S -wave interactions (without tensor coupling) by using an analytical continuation of the scattering wave function to the bound-state

pole of the S -matrix. For our purposes, we also require a similar relation for the virtual state. Thus, let us briefly reproduce the derivation from Ref. [15] with some minor changes in notations.

Near the pole $p = i\kappa$ corresponding to the bound or virtual state, the S -matrix can be presented in the form

$$S(p) = e^{2i\phi(p)} \approx -i \frac{N^2}{p - i\kappa}. \quad (9)$$

For a bound state, the constant N in Eq. (9) is a corresponding ANC (see [21, 22] and references therein). Near the pole, the relation (9) can also be written in the form

$$S(p) \approx 2\kappa \frac{N^2}{p^2 + \kappa^2}, \quad (10)$$

where $\kappa > 0$ for a bound state and $\kappa < 0$ for a virtual state.

The asymptotics of the wave function of both bound and virtual states in the configuration space can be written in a unified way:

$$u(r) \rightarrow N e^{-\kappa r}, \quad r \rightarrow \infty. \quad (11)$$

At the same time, the scattering wave function has the following asymptotics:

$$\psi_p(r) \rightarrow C^{(+)}(p) e^{ipr} - C^{(-)}(p) e^{-ipr}, \quad r \rightarrow \infty, \quad (12)$$

where in agreement with (8),

$$C^{(\pm)}(p) = \frac{e^{\pm i\phi(p)}}{\sqrt{2\pi i p}}. \quad (13)$$

Near the pole $p = i\kappa$, $\phi \rightarrow -i\infty$, $C^{(-)}(p) \rightarrow 0$; hence,

$$\psi_p(r) \rightarrow C^{(+)}(p) e^{-\kappa r}, \quad r \rightarrow \infty, \quad p \rightarrow i\kappa. \quad (14)$$

Comparing Eqs. (10) and (13), one can find an explicit relation between $C^{(+)}$ near the pole and ANC N :

$$\sqrt{\pi\kappa(p^2 + \kappa^2)} C^{(+)}(p) = -N. \quad (15)$$

The quantity

$$W(p, \kappa) = \sqrt{\pi\kappa(p^2 + \kappa^2)} \quad (16)$$

is referred to as the Fäldt-Wilkin's Factor (FWF).

Combining Eqs. (11), (14), and (15), we obtain the following relationship between the wave functions of the

discrete and continuous spectra

$$\lim_{p \rightarrow i\kappa} W(p, \kappa) \psi_p(r) = -u(r). \quad (17)$$

Equation (17) was derived in [15] for a bound state with $u(r)$ normalized to unity. However, we have just shown that it is also valid for the virtual state for which the wave function $u(r)$ is defined according to (11) with ANC N related to a pole of the S -matrix (9). The transition from a bound state to a virtual one can be considered as an analytical continuation with respect to the variable κ from $\kappa > 0$ to $\kappa < 0$, or equivalently, with respect to some constant characterizing the strength of the interaction potential.

Because $C^{(+)}(p)$ is real for imaginary values of p , it follows from (15) that ANC N is real for bound states ($\kappa > 0$) and purely imaginary for virtual states ($\kappa < 0$). The validity of this assertion can be illustrated by the example of the frequently used effective range approximation, within which

$$N = \sqrt{\frac{2\kappa}{1 - \kappa r_{\text{eff}}}}, \quad (18)$$

where r_{eff} is an effective range. Applying the effective range approximation to the np system in the 1S_0 -state and using the experimental values of the singlet scattering length ($a = -23.74$ fm) and effective range ($r_{\text{eff}} = 2.77$ fm) results in $\kappa = -0.0399$ fm⁻¹ and $N_v = i \cdot 0.268$ fm^{-1/2} ¹⁾.

C. Approximate relation for the momentum distributions

The relation (17) is an equality at the complex pole $p = i\kappa$ only. However, it should be approximately satisfied in a certain region near the pole, including small real positive p . Indeed, in [16], it was shown that a similar approximate relationship between the scattering function $\psi_p(r)$ at small p (low energies) and weakly bound state function $u(r)$ holds in the region of small values of r :

$$W(p, \kappa) \psi_p(r) \approx -u(r), \quad p \lesssim |\kappa|, \quad pr \ll 1. \quad (19)$$

A similar relation must also be valid for wave functions in the momentum representation, and thus for momentum distributions, in the high-momentum area for both bound and virtual states:

$$F(p, \kappa) |\psi_p(k)|^2 \approx |u(k)|^2, \quad p \lesssim |\kappa|, \quad k \gg p, \quad (20)$$

where the squared FWF is introduced as

$$F(p, \kappa) \equiv |W(p, \kappa)|^2 = \pi |\kappa| (\kappa^2 + p^2). \quad (21)$$

The approximation (20) can be explained as follows. The wave function of each type (*i.e.*, the bound state, virtual state, and scattering) satisfies the Schrödinger equation in the form:

$$\frac{\hbar^2}{2\mu} (k^2 - p^2) \psi_p(k) + \int_0^\infty \frac{dk' (k')^2}{2\pi^2} V(k, k') \psi_p(k') = 0, \quad (22)$$

where p is either an on-shell momentum (for the scattering wave function) or $p = i\kappa$ for the bound (virtual) state wave function. At $k \gg |p|$, the second term in parentheses on the left-hand side of Eq. (22) can be neglected. Therefore, the scattering and bound (or virtual) state wave functions for the same interaction potential should be the same at large momenta k up to some factor. According to (20), these factors are FWF for the wave functions and squared FWF for momentum distributions.

D. Case of coupled channels

The realistic NN interaction includes the tensor term, so the above S -wave formalism could not be applied directly for such a case. However, the approach can be generalized.

In particular, the total S -matrix is a matrix (2×2) for the coupled 3S_1 - 3D_1 channels. Near the bound-state pole $p = i\kappa_d$, it can be represented in the form [24, 25]

$$S(p) \approx -\frac{i}{p - i\kappa} \begin{pmatrix} N_S^2 & -N_S N_D \\ -N_S N_D & N_D^2 \end{pmatrix}, \quad (23)$$

where N_S and N_D are the ANCs introduced in Eq. (3). It can be shown that this S -matrix has one eigenvalue with a non-zero residue at $p = i\kappa_d$, corresponding to the so-called eigenchannel representation [25]. It seems that the procedure with a continuation to the bound-state pole can be applied and proved for one of the low-energy scattering states defined in this representation. Also note that at low positive energy, mixing in the S -matrix is very small; thus, the required momentum distribution can be calculated from the ordinary scattering wave function corresponding to the boundary condition with the incoming S -wave.

Thus, within the above assumptions, one can write the following approximate relation between the momentum distributions found from the scattering wave function and from the deuteron bound-state wave function in case of

1) It should be noted that in the work [23] a value for the ANC for a virtual np -state with the Yukawa potential $N_v = 0.268$ fm^{-1/2} was obtained, which differs from the one given above only by the absence of the factor i .

the realistic interaction:

$$F(p, \kappa_d) \sum_{l=0,2} |\psi'_{p,l}(k)|^2 \approx \rho_d(k), \quad p \lesssim \kappa_d, \quad k \gg p. \quad (24)$$

Here, we emphasize that this approximate equality should be valid only for one of the scattering states in the 3S_1 - 3D_1 channels at given on-shell momentum p , *i.e.*, the state corresponding to the incoming S -wave.

The approximate relations (20) and (24) between bound- and virtual-state momentum distributions and those found from the scattering wave functions represent the main result of this section. In fact, these relations allow us to obtain the high-momentum parts of the “basic” momentum distributions (2) and (6) from the low-energy scattering wave functions, as we have initially suggested. Prior to introducing a new form for the universal momentum distributions, in the next section, we will test both relations numerically in more detail.

III. CALCULATION OF THE MOMENTUM DISTRIBUTIONS FOR THE VIRTUAL STATES

In this section, we demonstrate that the approximations (20) and (24) are valid for cases of the model and realistic NN interactions.

A. Case of a separable potential

Using a simple example with a separable interaction, it is easy to test the considered approximations explicitly because all solutions are expressed in analytical form in this case. For the reader's convenience, we give the well-known formulas for a separable potential [26], but we supplement them with the details of the virtual state calculation, which seems to be less well-known.

Consider the S -wave attractive separable potential

$$V(k', k) = -\frac{\lambda}{2\mu} g(k')g(k), \quad \lambda > 0. \quad (25)$$

The unitary on-shell amplitude $f_0(p) \equiv 1/(p \cot \phi_0 - ip)$ is written in explicit form as

$$f_0(p) = \frac{\pi}{2} \frac{g^2(p)}{\lambda^{-1} + J(E)}, \quad (26)$$

where $E = p^2/(2\mu)$, μ is the reduced mass, and

$$J(E) = \int_0^\infty \frac{g^2(k)k^2 dk}{p^2 - k^2 + i0} = \text{Re}J(E) - \frac{i\pi p}{2} g^2(p). \quad (27)$$

The bound state function u_b for the separable potential (25) is found from the homogeneous Lippmann–

Schwinger equation (LSE) such that

$$u_b(k) = A_b \frac{g(k)}{\kappa^2 + k^2}, \quad E_b = -\frac{\kappa^2}{2\mu}, \quad (28)$$

where the normalization factor

$$A_b^{-2} = \int_0^\infty \frac{g^2(k)k^2 dk}{(\kappa^2 + k^2)^2}, \quad (29)$$

and the energy E_b is determined by the condition

$$\lambda^{-1} = -J(E_b) = \int_0^\infty \frac{g^2(k)k^2 dk}{\kappa^2 + k^2}. \quad (30)$$

The bound state exists for $\lambda > \lambda_{\min}$ ($\lambda_{\min} = \{\int_0^\infty g^2(k)dk\}^{-1}$ corresponds to $\kappa = 0$), while for $\lambda < \lambda_{\min}$, there is a virtual state with $\kappa < 0$, which corresponds to the pole of the t -matrix on the unphysical energy sheet.

The virtual state must satisfy the LSE continued to the second (unphysical) sheet of the energy Riemann surface (or for $\text{Im } p < 0$). As shown, for example, in [20], the continuation to the second energy sheet is actually a continuation of the Cauchy-type integral and reduces to adding a separable energy-dependent term to the interaction. For the case of an initial separable potential, this is equivalent to modifying the coupling constant λ .

Therefore, in the case of a separable potential, the formulas for determining the functions on the second energy Riemann sheet remain the same those on the physical sheet, but a residue at the pole $p = -i|\kappa|$ (multiplied by $2i\pi$) must be added to all integrals over k , including the factor $1/(p^2 - k^2)$. In particular, Eq. (30) relating λ and κ for the virtual state takes the form

$$\lambda_v^{-1} = \int_0^\infty \frac{g^2(k)k^2 dk}{\kappa^2 + k^2} + \pi g^2(-i|\kappa|)|\kappa|. \quad (31)$$

In this case, the virtual state function itself in the momentum representation has the same form as the bound state function (28):

$$u_v(k) = A_v \frac{g(k)}{\kappa^2 + k^2}, \quad (32)$$

i.e., it is square-integrable (unlike the function in the coordinate representation). However, when calculating the normalization factor for this function, a residue (of the second order) at the pole $p = -i|\kappa|$ must be added to the integral:

$$A_v^{-2} = \int_0^\infty \frac{g^2(k)k^2 dk}{(\kappa^2 + k^2)^2} + 2i\pi \text{Res} \left\{ \frac{g^2(p)p^2}{(\kappa^2 + p^2)^2} \right\} \Big|_{p=-i|\kappa|}. \quad (33)$$

Here, there is no need to use explicit formulas (32) or (33) to continue Cauchy-type integrals, as these integrals are given by analytical functions. Having calculated the integral in (30) for positive κ , one gets the analytic function $\lambda^{-1}(\kappa)$, which is defined for any values κ and thus determines the value of λ^{-1} corresponding to the bound (for $\kappa > 0$) or virtual state (for $\kappa < 0$). The same applies to the normalization factor (29).

Below, we present some results for the Yamaguchi form factor [26]:

$$g(k) = \frac{1}{k^2 + \beta^2}, \quad (34)$$

for which the explicit relations are well known in both configuration and momentum representations. In particular, the integrals (30) and (29) for the Yamaguchi form factor define functions

$$\lambda^{-1}(\kappa) = \frac{\pi}{4\beta(\kappa + \beta)^2}, \quad A_{b(v)}^{-2}(\kappa) = \frac{\pi}{4\beta\kappa(\kappa + \beta)^3}, \quad (35)$$

which are analytic in the entire κ -plane except for the pole at $\kappa = -\beta$. It should be noted that according to (35), the square of the normalization factor A_v^2 for the virtual state function ($\kappa < 0$) is negative, *i.e.*, the virtual state function $u_v(k)$ and its ANC are purely imaginary (cf. (18)). The wave function of the bound (or virtual) state for the Yamaguchi potential in configuration space has a very simple form:

$$u_{b(v)}(r) = N_{b(v)}(e^{-\kappa_{b(v)}r} - e^{-\beta r}). \quad (36)$$

Note that the wave function (36) coincides with the wave function for the local Hulthén potential: $V(r) = -V_0 e^{-\beta r}/(1 - e^{-\beta r})$.

It is easy to show that the ANC $N_{b(v)}$ for a separable potential is expressed in terms of the normalizing factor $A_{b(v)}$ and the value of the form factor at the pole $g(i\kappa)$:

$$N_{b(v)} = \sqrt{\frac{\pi}{2}} A_{b(v)} g(i\kappa) = \frac{\sqrt{2\kappa\beta(\beta + \kappa)}}{\beta - \kappa}. \quad (37)$$

The S -wave scattering function $|\psi_p^+\rangle$ for energy $E = p^2/2\mu$ can be written in an explicit form, *e.g.*, in terms of the amplitude $f_0(p)$ (26):

$$\psi_p^+(k) = \frac{\delta(p - k)}{p^2} - \frac{g(k)}{p^2 + i\varepsilon - k^2} \frac{\frac{2}{\pi} f_0(p)}{g(p)}. \quad (38)$$

Let us now check the approximations (20) and (24). We use the Yamaguchi potential [26] with the parameter $\beta = 1.4488 \text{ fm}^{-1}$ and two values of κ corresponding to two

main NN -configurations (at $\hbar^2/2\mu = 41.47 \text{ MeV fm}^2$): $\kappa = -0.04045 \text{ fm}^{-1}$, which corresponds to the singlet NN -channel with a virtual state, and $\kappa = 0.2316 \text{ fm}^{-1}$, which gives a bound state with $E_b = -2.2244 \text{ MeV}$.

Figure 1 shows the momentum distributions for the scattering wave functions $\rho_p(k) = F(p, \kappa) |\psi_p(k)|^2$, calculated for the two above-mentioned values of κ and three energies corresponding to the values of the on-shell momentum: $p = 0, 0.06$, and 0.12 fm^{-1} in comparison with the momentum distributions for the virtual state $|u_v(k)|^2$ and bound state $|u_b(k)|^2$.

As can be seen from Fig. 1, the momentum distributions $\rho_p(k) = F(p, \kappa) |\psi_p(k)|^2$ found from the low-energy scattering wave functions do not depend on p at $k > p$ and approach (in absolute value) the corresponding momentum distribution for the virtual or bound state. Thus, the approximation based on the Fäldt–Wilkin equality does indeed work in the region of large momenta for both the bound and virtual states. Note that, as discussed above, a chosen form of the virtual state wave function means that the integral $\int_0^\infty |u_v(k)|^2 k^2 dk$ is not equal to unity in contrast to the bound-state. For example, such an integral of $|u_v(k)|^2$ with $\kappa = -0.04045 \text{ fm}^{-1}$, as shown in Fig. 1, is equal to 0.8377.

To demonstrate the accuracy of the approximation (20), Fig. 2 shows the ratios of the momentum distributions $\rho_p(k)$ at different p to the virtual-state momentum distribution $\rho_v(k)$. This ratio has the form

$$R_{p,\kappa}(k) = \frac{\rho_p(k)}{\rho_v(k)} = A(\kappa, p) \chi_{p,\kappa}(k), \quad (39)$$

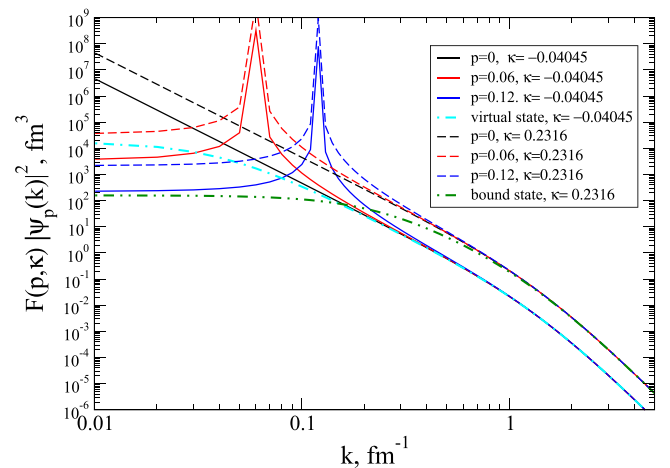


Fig. 1. (color online) Momentum distributions for the scattering functions $\rho_p(k) = F(p, \kappa) |\psi_p(k)|^2$ for the Yamaguchi potential at three values $p = 0, 0.06$, and 0.12 fm^{-1} and for two values of κ : -0.04045 fm^{-1} (solid curves) and $\kappa = 0.2316 \text{ fm}^{-1}$ (dashed curves) compared to the momentum distributions for the virtual state $|u_v(k)|^2$ and bound state $|u_b(k)|^2$.

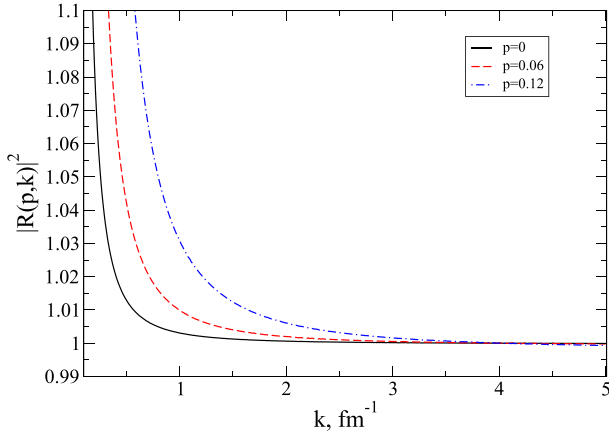


Fig. 2. (color online) Ratio of momentum distributions for the scattering functions $\rho_p(k) = F(p, \kappa) |\psi_p(k)|^2$ at $p = 0, 0.06$, and 0.12 fm^{-1} to the distribution for the virtual state $|u_v(k)|^2$ at $\kappa = 0.04045 \text{ fm}^{-1}$.

where the function determining k dependence

$$\chi_{p,\kappa}(p) = \left(\frac{k^2 + \kappa^2}{k^2 - p^2} \right)^2 + 2 \frac{\kappa^2 + p^2}{k^2}, \quad k \gg p, \kappa. \quad (40)$$

monotonically approaches 1 (the faster it does, the smaller $\kappa^2 + p^2$). At the same time, the ratio $R_{p,\kappa}(k)$ tends to the limit value $A(\kappa, p)$, which is slightly less than 1, even at zero energy $p = 0$, due to the non-zero value of κ .

The limit values $A(\kappa, p)$ for $\kappa = -0.0405 \text{ fm}^{-1}$ are 0.9998, 0.9994, and 0.9980 for $p = 0, 0.06$, and 0.12 fm^{-1} , respectively. For comparison, the limit ratio $A(\kappa, 0)$ at $\kappa = 0.2316 \text{ fm}^{-1}$, corresponding to the bound state, is 0.9971. As can be seen from Fig. 2, at $p = 0$, the ratio $R_{p,\kappa}(k)$ differs from 1 by less than one percent for all $k > 0.6 \text{ fm}^{-1}$. The above accuracy of the approximation (20) seems to be sufficient for calculations with such two-nucleon momentum distributions.

B. Approximations (20) and (24) for a realistic NN potential.

Let us now test the approximations based on the Fäldt–Wilkin factor for a realistic local NN interaction. In Fig. 3, we present the momentum distributions for the 1S_0 np scattering wave functions with the factor (21) at three values of energy for the Argonne V18 (AV18) potential [27]. Here, the wave number of the virtual state is $\kappa_v = -0.04 \text{ fm}^{-1}$. All three curves in this figure are almost indistinguishable in the region $k > 1 \text{ fm}^{-1}$. Thus, the FWF indeed allows us to get close momentum distributions at different small on-shell momenta. Based on the exact equality (17) and the results for separable interaction, we assume that the approximation (20) is also valid for realistic interaction. That is, the momentum distribution for the scattering state multiplied by the factor (21) is an ap-

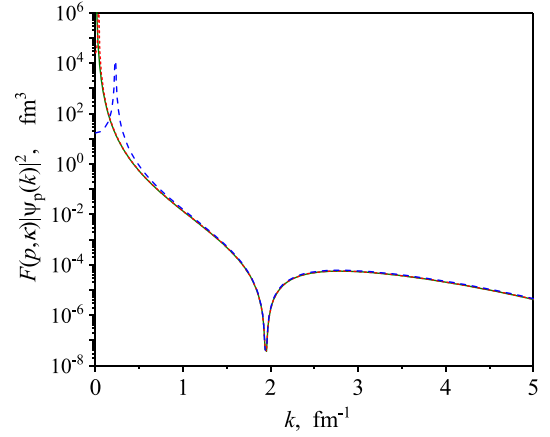


Fig. 3. (color online) Spin-singlet np momentum distributions for the AV18 potential with the factor from Eq. (20) for three momenta: $p = 0.008 \text{ fm}^{-1}$ (solid curve), $p = 0.041 \text{ fm}^{-1}$ (dotted curve), and $p = 0.23 \text{ fm}^{-1}$ (dashed curve).

proximation of the momentum distribution for the virtual state in this case.

In Fig. 4, we test the relation (24) for the 3S_1 – 3D_1 coupled channels with AV18 NN interaction. Here, $\kappa_d = 0.2316 \text{ fm}^{-1}$. Although all three curves are very close to each other in the high- k region, one can see a small deviation of the momentum distributions found from the scattering wave functions from the deuteron one, even for the smallest p . Thus, the approximate relation (24) is also valid for realistic NN -interaction. Here, we can even estimate its error, which is approximately 5% for the case of zero energy.

Taking into account the above example with a separable potential, it can be concluded that the FWF-based approximation works slightly better for the spin-singlet channel due to the smaller value of $|\kappa|$. Thus, the error for

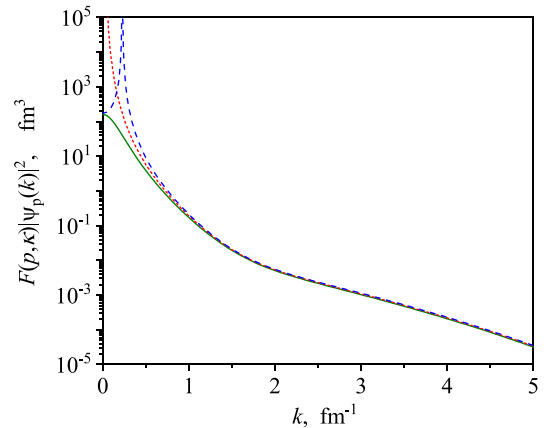


Fig. 4. (color online) Deuteron momentum distribution (solid curve) for AV18 potential in comparison with the momentum distributions found from the scattering wave functions according to Eq. (24): $p = 0.041 \text{ fm}^{-1}$ (dotted curve) and $p = 0.23 \text{ fm}^{-1}$ (dashed curve).

the spin-singlet channel should be no more than 2%–3%.

IV. UNIVERSAL MOMENTUM DISTRIBUTIONS AND THEIR PROPERTIES

A. Universal momentum distributions based on the virtual states

The results of the previous sections allow us to introduce a new form for UMD for the singlet NN channels based on the scattering wave functions at zero or small on-shell momentum p as follows:

$$\rho_p^s(k) = F(p, \kappa_v) |\psi_p^s(k)|^2. \quad (41)$$

Based on the results of the previous sections, in the high-momentum region, these distributions should approximate the momentum distribution for the virtual state (6) (whose wave function in the configuration space is uniquely determined by the ANC (5)):

$$\rho_p^s(k) \approx \rho_v(k), \quad p \lesssim \kappa_v, \quad k \gg p. \quad (42)$$

Here, it should be noted that for the interactions that take the charge dependence of NN forces into account, one will have three different singlet UMDs for pp , np , and nn pairs. The values of κ_v differ for these three cases as well.

The corresponding UMD for the spin-triplet channel is just the deuteron momentum distribution. A comparison of the deuteron momentum distributions for different NN interactions is presented in Fig. 5. Below, we consider four models for NN interactions: CD Bonn potential [28], AV18 potential [27] and two versions of the dibaryon model with energy dependent interactions, DBM-1 and DBM-2024 (see details and further Refs. in [29]). As shown in Fig. 5, the deuteron momentum distributions at small relative momenta are nearly indistinguishable for the considered interactions, while in the high-momentum region, at $k > 1.3 \text{ fm}^{-1}$, all distributions show quite different behavior. Thus, we chose the above interactions with evidently different high-momentum properties for further tests of the presented formalism.

A comparison of the spin-singlet np UMDs constructed from the scattering wave functions (calculated at $p = 0.008 \text{ fm}^{-1}$) using (41) for the four above interactions is shown in Fig. 6.

It can be seen that the UMDs for different interactions are almost the same in the momentum region $0.2 < k < 0.6 \text{ fm}^{-1}$. Also, in this region, they are close to the exact distribution $\rho_v(k)$ for the separable Yamaguchi potential, as shown by dots. At the same time, at $k > 1 \text{ fm}^{-1}$, all distributions exhibit different behavior, which is primarily due to the difference in the position of the

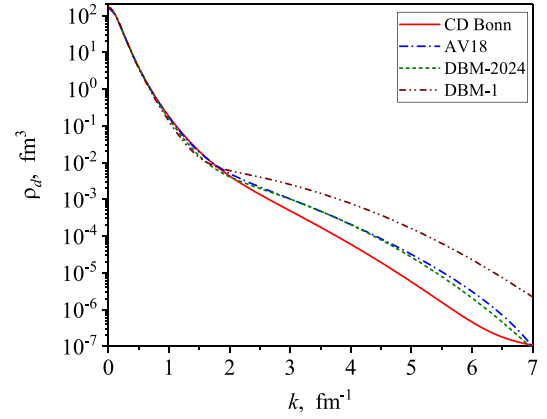


Fig. 5. (color online) Spin-triplet (deuteron) np -momentum distributions for different realistic NN -potentials: CD Bonn (solid curve), AV18 (dash-dotted curve), DBM-2024 (dashed curve), and DBM-1 (dash-dot-dotted curve).

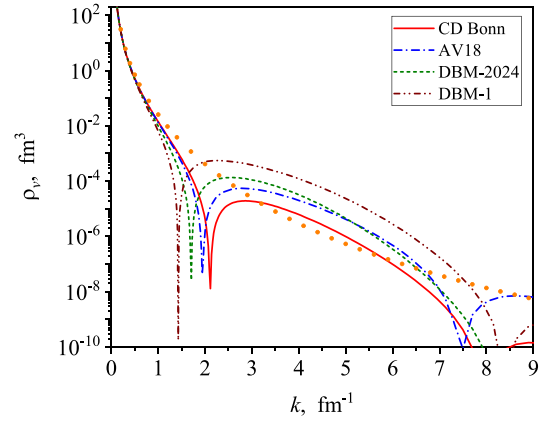


Fig. 6. (color online) Spin-singlet np universal momentum distributions for different realistic NN -potentials. The notations are the same as in Fig. 5. The dots show the virtual-state momentum distribution for the Yamaguchi potential.

nodes of the corresponding wave functions.

Thus, by using the definition of (41), one can evidently compare high-momentum components of the distributions in the spin-singlet channels for different NN interactions. Below, we introduce constants that allow us to quantify these differences.

B. High-momentum components of the UMDs

To consider high-momentum parts of the distributions, which just correspond to SRC, let us introduce the boundary of the high-momentum region as a constant p_0 . Usually, it is taken to be comparable with the Fermi momentum k_F in nuclei [5, 13].

A high-momentum part of the deuteron (bound-state) distribution is defined by the integral

$$a_2^d = \int_{p_0}^{\infty} dk k^2 \rho_d(k), \quad (43)$$

which, due to normalization to unity (2), is simply the weight of the high-momentum components in the deuteron. The values of a_2^d are different for different realistic NN -interactions [13].

Now, one can consider the high-momentum parts of the singlet UMDs by taking the integral of the momentum distribution for the virtual state (6):

$$a_2^v \equiv \int_{p_0}^{\infty} dk k^2 \rho_v(k). \quad (44)$$

It should be emphasized that, unlike the triplet channel, the quantity a_2^v is not the weight of the high-momentum tail in the singlet channel. However, the quantity a_2^v is dimensionless, and its value estimates the high-momentum contribution for different NN interactions.

For practical calculation of these quantities, let us consider high-momentum integrals of the squared modulus of scattering wave functions:

$$\begin{aligned} c_2^s(p) &= \int_{p_0}^{\infty} dk k^2 |\psi_p^s(k)|^2, \\ c_2^t(p) &= \sum_{l=0,2} \int_{p_0}^{\infty} dk k^2 |\psi_{p,l}^t(k)|^2, \end{aligned} \quad (45)$$

where $p \ll p_0$ is assumed so that these integrals are finite. The functions $c_2^{s(t)}(p)$ do not have the same meaning as the values a_2^d and a_2^v , as is already evident from their dimension (fm^3); however, they contain quantitative information about the high-momentum components of the NN scattering states.

By using FWF, one can get an explicit approximate expression for the constant a_2^v for a virtual state:

$$a_2^v \approx c_2^s(p) F(p, \kappa_v), \quad p \ll p_0, \quad p \lesssim |\kappa_v|. \quad (46)$$

The same approximate equality is also valid for the triplet channel, but there is no need for it there, as the high-momentum constant a_2^d is simply calculated from the deuteron momentum distribution.

To check the relation (46), Fig. 7 shows the function $c_2^s(p)F(p, \kappa_{np})$ for the NN potentials considered here. As can be seen from the figure, these functions are practically constant at $p < 0.1 \text{ fm}^{-1}$, which allows us to calculate the values a_2^v for different potentials from the scattering wave functions.

The values of a_2^v for different NN interactions in comparison with a_2^d found for the deuteron momentum distribution are given in Table 1. Here, the high-momentum region boundary $p_0 = 1.4 \text{ fm}^{-1}$ is used, which corresponds to the generally accepted value of k_F for nuclei. From Table

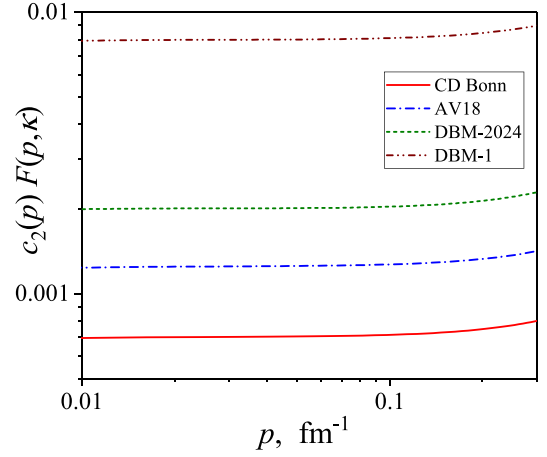


Fig. 7. (color online) Function $c_2^s(p)$ with the factor (21) at low on-shell momentum p for different np potentials.

Table 1. High-momentum constants for different NN models for $p_0 = 1.4 \text{ fm}^{-1}$.

model	a_2^d	$a_2^{v(np)}$	$a_2^{v(pp)}$	$a_2^{v(pp)}/a_2^d$
CD Bonn	0.031	0.0007	0.0009	0.03
AV18	0.041	0.0013	0.0016	0.04
DBM-2024	0.036	0.002	0.0026	0.07
DBM-1	0.068	0.008	0.011	0.16

1, it can be seen that the spread of high-momentum constants for various interactions is different for triplet and singlet channels. In all cases, even for the traditional AV18 and CD Bonn models, the a_2^v constants differ from each other more than the a_2^d constants for the same potentials.

Note also that the a_2^d value for DBM-2024 is slightly smaller than that for AV18, while the a_2^v values are more than 1.5 times larger than for AV18. Thus, one can conclude that the value a_2^v represents an independent high-momentum characteristic of the NN interaction in spin-singlet channels.

In Table 1, the high-momentum constants for the pp interaction, $a_2^{v(pp)}$, are also presented. These constants correspond ¹⁾ to $\kappa_{pp} \approx -0.054 \text{ fm}^{-1}$. It is clear that the ratio $a_2^{v(pp)}/a_2^{v(np)}$ depends very weakly on the model.

Finally, in Table 1, we present the ratios of constants $a_2^{v(pp)}/a_2^d$, which are discussed in the next subsection.

C. Two-body estimations for pp/np ratios

Recently [18], we proposed a way to calculate the weight of high-momentum components for scattering wave functions via the integral over on-shell momentum p up to some small value q ($q \ll p_0$):

1) Here the Coulomb interaction between protons is not taken into account.

$$A_{s(i)}(q) = \int_0^q dp p^2 c_2^{s(i)}(p). \quad (47)$$

Such an integral is dimensionless and can be compared with the a_2^d value for the bound-state wave function.

Now, one can also quantitatively compare the weights of high-momentum components for the singlet and triplet channels using the ratio [18]

$$\eta(q) = A_s(q)/(a_2^d + A_t(q)). \quad (48)$$

The values in the numerator and denominator represent the cumulative weights of high-momentum components from all states of the spectra up to the energy related to the considered on-shell momentum q in the singlet and the triplet NN channels, respectively.

Using the relations in (46) as approximations for both singlet and triplet functions $c_2(p)$ at small values of p , one gets the following approximate expressions for the high-momentum integrals $A(q)$ at small q :

$$A^{s(i)}(q) \approx \frac{a_2^{v(d)}}{\pi} \gamma(q/|\kappa_{v(d)}|), \quad \gamma(x) \equiv x - \arctan x. \quad (49)$$

This results in the following relation for the ratio $\eta(q)$:

$$\eta(q) \approx \frac{a_2^v}{a_2^d} \zeta\left(\frac{q}{|\kappa_v|}, \frac{q}{\kappa_d}\right), \quad \zeta \equiv \frac{\gamma(q/|\kappa_v|)}{\pi + \gamma(q/\kappa_d)}. \quad (50)$$

A useful feature of this presentation is that the function ζ depends on the on-shell parameters κ_v and κ_d only, so the dependence on q in the ratio η is the same for all the realistic NN interactions. Thus, the only difference in the values of $\eta(q)$ for different NN interaction models is the ratio of the constants a_2^v/a_2^d . At $q = |\kappa_{pp}|$ and $q = \kappa_d$, the corresponding ratios are as follows:

$$\eta(|\kappa_{pp}|) \approx 0.07 \frac{a_2^{v(pp)}}{a_2^d}, \quad \eta(\kappa_d) \approx 0.89 \frac{a_2^{v(pp)}}{a_2^d}. \quad (51)$$

One can see that the ratio of high-momentum weights $\eta(q)$ increases with increasing q , showing that the spin-singlet channel contribution to high-momentum components grows faster with energy than the spin-triplet one. At the same time, the ratio $a_2^{v(pp)}/a_2^d$ represents an informative characteristic for high-momentum components of the momentum distributions in continuum for the chosen model of the NN interaction.

Using the data from Table 1, one can compare the ratios $a_2^{v(pp)}/a_2^d$ at $p_0 = 1.4 \text{ fm}^{-1}$ for different NN interactions. From the considered models, the minimal value of this ratio corresponds to the CD Bonn potential, while the DBM-1 gives an essentially greater one. Based on the contact formalism, we may also expect that the use of an

interaction with greater a_2^v/a_2^d ratio at the two-nucleon level will lead to greater mean values for the ratios of pp and np momentum distributions in nuclei.

Figure 8 presents the ratio $a_2^{v(pp)}/a_2^d$ as a function of the high-momentum parameter p_0 . One can see that the ratio $a_2^{v(pp)}/a_2^d$ depends significantly on the value of p_0 . It is interesting to note that the minimum of this ratio for the conventional AV18 and CD Bonn potentials corresponds just to the most frequently considered range of $p_0 \sim 1.3 - 1.5 \text{ fm}^{-1}$, where the pp/np ratio is very sensitive to the chosen value of p_0 .

Thus, the UMDs suggested in this section are quite convenient for practical calculations. The developed formalism also allows a high-momentum constant a_2^v to be introduced for the spin-singlet channel, in addition to a_2^d for the deuteron channel. Besides, some estimations for the ratios of pp and np momentum distributions in nuclei for various models of NN interactions can already be given at the two-body level. In the next section, we show how the introduced UMDs can be employed within the contact formalism for analyzing NN distributions in ^3He .

V. TWO-NUCLEON DISTRIBUTIONS IN ^3He

Here, we test the factorization property (1) of two-nucleon momentum distributions ρ_{NN}^A for the ^3He nucleus as an example and calculate the nuclear contacts $C_{NN}^{^3\text{He}}$ for various interactions. We consider the distributions $\rho_{NN}^A(k, Q = 0)$, which correspond just to back-to-back SRC pairs, where Q is the center-of-mass momentum of the pair.

In this case, it is convenient to introduce the normalized distribution at $Q = 0$ as follows [9]:

$$\rho_{NN}^0(k) = \frac{\rho_{NN}^A(k, Q = 0)}{\rho_{cm}^{A,NN}(Q)|_{Q=0}}, \quad \int_0^\infty \rho_{NN}^0(k) k^2 dk = n_{NN}, \quad (52)$$

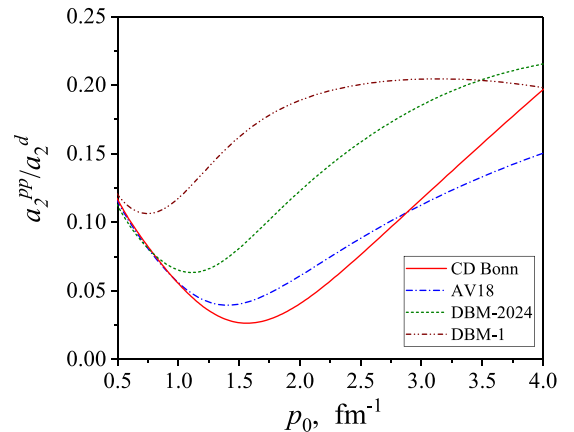


Fig. 8. (color online) Ratio of $a_2^{v(pp)}/a_2^d$ values as a function of high-momentum parameter p_0 for different NN potentials.

where n_{NN} is a number of nucleon pairs, which is equal to 2 for $NN = np$ and 1 for $NN = pp$. Note that with such a normalization, the distribution of the center-of-mass momentum of a pair of nucleons $\rho_{cm}^{A,NN}(Q)$ is assumed to be normalized to 1.

According to [9], the normalized momentum distribution is proportional to the UMD $\rho_{NN}(k)$ in the high-momentum region, with the nuclear contact as a factor:

$$\rho_{NN}^0(k) \approx C_{NN} \rho_{NN}(k), \quad k > p_0. \quad (53)$$

Here, because we consider only the ${}^3\text{He}$ nucleus, we have omitted the index A , indicating the nucleus, in the notations of the distributions ρ and nuclear contacts C . Below, we use the UMDs $\rho_{np} = \rho_d$ and $\rho_{pp} = \rho_{v(pp)}$ for np - and pp -pairs, respectively.

We use the same four NN interactions: CD Bonn, AV18, DBM-1, and DBM-2024 listed in the previous section and the ${}^3\text{He}$ NN -distributions calculated using these interactions and corresponding three-particle forces. The ${}^3\text{He}$ distributions for AV18 potential with UIX $3N$ force are taken from Ref. [30], the distributions for CD Bonn potential supplemented with $3N$ TM force are from Ref. [13], and the distributions for the two versions of the DBM were obtained by the present authors from the variational calculations on an antisymmetrized Gaussian basis (see details in Ref. [29]).

First, let us check how the factorization (53) is satisfied for np distributions, where the momentum distribution in the deuteron is used as the UMD. Figure 9 shows the normalized momentum np -distributions in ${}^3\text{He}$ at $Q = 0$, $\rho_{np}^0(k)$, for the different interaction models in comparison with the corresponding deuteron distributions $\rho_d(k)$ multiplied by the corresponding nuclear contacts C_{np} .

Here, for all the interaction models considered, the ${}^3\text{He}$ momentum distributions achieve the deuteron "asymptotics" already at the relative momentum $k \sim 1.5 \text{ fm}^{-1}$. Although high-momentum parts of the distributions for different interactions differ significantly, their ratios to their "own" deuteron momentum distributions in the high-momentum region (*i.e.*, the nuclear contacts) are nearly independent of the interaction model. The found nuclear contacts C_{np} for all considered interaction models are close to 2, which agrees with the results of Ref. [9]. The values of C_{np} found in the present study are given in Table 2.

Now, having the UMD for the singlet channel $\rho_v(k)$, one can compare the normalized momentum pp -distributions in ${}^3\text{He}$ at $Q = 0$ with these UMDs and find the corresponding nuclear contacts C_{pp} . Figure 10 shows such a comparison for the four interaction models considered. Here, the ratios of the pp -distributions to the corresponding UMDs become nearly constant at values of $k \geq 2.3$

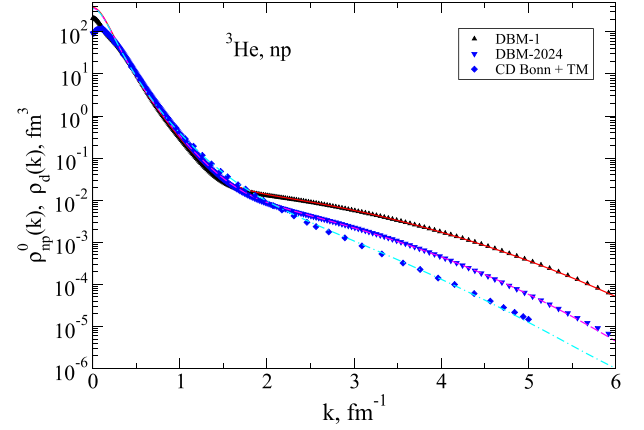


Fig. 9. (color online) Normalized momentum np -distributions in ${}^3\text{He}$ at $Q = 0$, $\rho_{np}^0(k)$, for three interaction models (DBM-1 – triangles-up, DBM-2024 – triangles-down, CD Bonn+TM – diamonds) in comparison with the corresponding deuteron distributions $\rho_d(k)$ multiplied by C_{np} (solid curves).

Table 2. Nuclear contacts for ${}^3\text{He}$ for different models of NN and $3N$ interaction.

	AV18 + UIX	CD Bonn + TM ^a	DBM-1	DBM-2024
C_{np}	1.82 ± 0.07	2.2	2.26 ± 0.03	2.17 ± 0.04
C_{pp}	2.91 ± 0.16	3.1	3.12 ± 0.03	2.98 ± 0.05

^aThe data on the distribution in ${}^3\text{He}$ are obtained by digitizing the figure in Ref. [13] so that the results are given without errors.

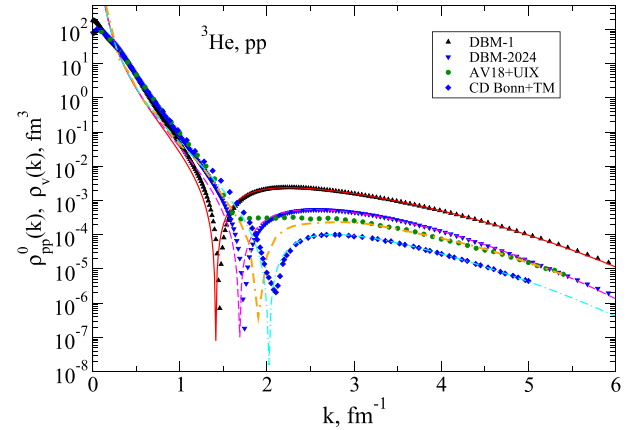


Fig. 10. (color online) Normalized momentum pp distributions in ${}^3\text{He}$ at $Q = 0$, $\rho_{pp}^0(k)$, for four interaction models in comparison with the corresponding singlet UMDs, multiplied by the contacts C_{pp} . The notations are the same as in Fig. 9, with filled circles representing AV18+UIX.

fm^{-1} . In this figure, we show the UMDs multiplied by the corresponding nuclear contacts C_{pp} , the values of which are given in Table 2 and are close to 3.

As mentioned above, the values of the nuclear contacts found for the np -pairs are consistent with the results of Ref. [9]. However, these values of both np - and

pp -nuclear contacts differ from those given in Ref. [5] because the definitions of the corresponding UMDs and nuclear contacts are different there¹⁾ (see also the relations between momentum distributions in Appendix A).

Thus, we have shown that the nuclear contacts for the ${}^3\text{He}$ nucleus, calculated with respect to the two-particle UMD corresponding to a virtual state, are indeed almost identical for NN interactions; nevertheless, the high-momentum components of the momentum distributions for those interactions differ significantly at $k > p_0$. Based on the results of the contact formalisms [5, 9], one may expect that this property will hold for heavier nuclei.

VI. SUMMARY

In this paper, we have suggested a way to construct the momentum distributions for the spin-singlet 1S_0 NN channels based on the virtual state from the low-energy scattering wave functions. The advantages of such momentum distributions are as follows:

(i) The distribution does not depend on the boundary of the high-momentum region p_0 .

(ii) One can introduce two-nucleon short-range constants a_2^v for spin-singlet channels, which characterize the NN interaction with respect to high-momentum components of wave functions, similar to the value a_2^d , which is well known for the deuteron channel.

(iii) The ratio $a_2^{v(pp)}/a_2^d$ differs for various realistic NN models and allows us to estimate differences in ratios of pp - and np -momentum distributions in nuclei.

(iv) In the low-momentum region, the momentum distribution for the virtual state depends only on the on-shell characteristics of the NN -system, such as the wave number κ and scattering length, which are the same for all realistic NN interaction models. Thus, the introduced UMDs turn out to be the same for different models in the momentum region of $0.2\text{--}0.6\text{ fm}^{-1}$, exhibiting obvious differences at high momenta.

(v) Due to the previous property, the nuclear contacts calculated relative to the introduced UMDs should be nearly the same for different realistic NN interactions.

The last property has been demonstrated for $A = 3$ nuclei with four essentially different models of NN interactions, which correspond to the same observables in $2N$ and $3N$ systems. One can expect that a weak dependence of nuclear contacts on the NN interaction will also hold for heavier nuclei, which should be studied and verified

in future research.

The above conclusion seems to differ from the results of Ref. [5], where a spread of the pp -nuclear contacts for different NN interactions was found. This is caused by the difference in the definitions of UMDs and nuclear contacts. At the same time, the relation (A5) from Appendix A shows that the ratio of nuclear contacts for two nuclei remains the same for differently defined UMDs. This result agrees with the findings of Ref. [5], where a very weak dependence on the interaction models for such ratios of the nuclear contacts was demonstrated.

The suggested spin-singlet universal distributions based on the momentum distribution for the virtual state can be considered as a supplement to the contact formalism presented in Ref. [9] for the triplet np distributions. Because the proposed UMDs do not depend on the high-momentum boundary p_0 , one can expect that our formalism will be suitable for calculations with NN models using various "low- k " approximations. In particular, the nuclear pp -contacts for such interactions would be the same as for other realistic NN models, as the momentum distributions for the virtual state are nearly identical at low momenta for all realistic NN interactions. One may assume that the contacts will not depend on the cut-off parameters for this type of NN potentials as well.

APPENDIX A. RELATION BETWEEN DIFFERENT UNIVERSAL DISTRIBUTIONS

Let us show how the introduced UMDs are related to other universal distributions used in the GCF.

The momentum distribution for the virtual state can be calculated using the scattering wave function at zero energy $\psi_{p=0}^s(k)$ (normalized according to (7)) from the relation

$$\rho_v(k) \approx \pi |\kappa_v|^3 |\psi_{p=0}^s(k)|^2, \quad (\text{A1})$$

which is valid with high accuracy at $k > 0.5\text{ fm}^{-1}$.

The universal momentum distributions normalized to unity in the region $[p_0, \infty)$ can be calculated from the ratios [18]

$$\bar{\rho}_p^s(k) = \frac{|\psi_p(k)|^2}{c_2^s(p)}, \quad \bar{\rho}_p^t(k) = \frac{\sum_{l=0,2} |\psi_{p,l}^t(k)|^2}{c_2^t(p)}, \quad (\text{A2})$$

where functions $c_2(p)$ are defined in Eq. (45). It has been shown [18] that these distributions do not depend on p in the high-momentum region.

Thus, by using Eq. (46) for the spin-singlet channel, one gets that such a "tail-normalized" distribution is re-

1) The nuclear contacts in GCF are defined for the momentum distributions integrated over the center of mass momentum Q .

lated to the density defined in Eq. (41) as follows:

$$\bar{\rho}_p^s(k) = \rho_p^s(k)/a_2^s, \quad (\text{A3})$$

which can be used at $p = 0$ as well. At the same time, the nuclear contacts defined relatively these two types of the universal distributions are recalculated as follows:

$$\bar{C}_{pp}^A = a_2^{v(pp)} C_{pp}^A, \quad (\text{A4})$$

where \bar{C}_{pp}^A is a nuclear contact corresponding to the distribution $\bar{\rho}$. This property shows that the ratios of the nuclear contacts for two nuclei A_1 and A_2 are the same for both distributions:

$$\frac{\bar{C}_{pp}^{A_1}}{\bar{C}_{pp}^{A_2}} = \frac{C_{pp}^{A_1}}{C_{pp}^{A_2}}. \quad (\text{A5})$$

References

- [1] M. Duer *et al.* (CLAS collaboration), *Nature* **560**, 617 (2018)
- [2] S. Li, R. Cruz-Torres, N. Santiesteban *et al.*, *Nature* **609**, 41 (2022)
- [3] C. Ciofi degli Atti, *Phys. Rep.* **590**, 1 (2015)
- [4] J. Arrington, N. Fomin, and A. Schmidt, *Annu. Rev. Nucl. Part. Sci.* **72**, 307 (2022)
- [5] R. Cruz-Torres, D. Londeroni, R. Weiss *et al.*, *Nat. Phys.* **17**, 306 (2021)
- [6] R. Subedi, R. Shneor, P. Monaghan *et al.*, *Science* **320**, 1476 (2008)
- [7] I. Korover, N. Muangma, O. Hen *et al.*, *Phys. Rev. Lett.* **113**, 022501 (2014)
- [8] I. Korover, J. R. Pybus, A. Schmidt *et al.* (CLAS collaboration), *Phys. Lett. B* **820**, 136523 (2021)
- [9] M. Alvioli, C. Ciofi degli Atti, and H. Morita, *Phys. Rev. C* **94**, 044309 (2016)
- [10] R. Weiss, R. Cruz-Torres, N. Barnea *et al.*, *Phys. Lett. B* **780**, 211 (2018)
- [11] R. Schiavilla *et al.*, *Phys. Rev. Lett.* **98**, 132501 (2007)
- [12] C. Ciofi degli Atti and H. Morita, *Phys. Rev. C* **96**, 064317 (2017)
- [13] F. Sammarruca, *Phys. Rev. C* **92**, 044003 (2015)
- [14] Yu. N. Uzikov and A. Uvarov, *Phys. Part. Nucl.* **53**, 426 (2022)
- [15] G. Fäldt and C. Wilkin, *Phys. Scrip.* **56**, 566 (1997)
- [16] G. Fäldt and C. Wilkin, *Amer. J. Phys.* **66**, 876 (1998)
- [17] G. Fäldt and C. Wilkin, *Phys. Lett. B* **382**, 209 (1996)
- [18] O. A. Rubtsova and V. N. Pomerantsev, *JETP Lett.* **120**, 547 (2024)
- [19] E. Hernández and A. Mondragón, *Phys. Rev. C* **29**, 722 (1984)
- [20] Yu. V. Orlov and V. V. Turovtsev, *Sov. Phys. JETP* **59**, 934 (1984)
- [21] A. I. Baz, Ya. B. Zeldovich, and A. M. Perelomov, *Scattering, Reactions and Decay in Nonrelativistic Quantum Mechanics*, Second edition (Nauka, Moscow, 1971, in Russian) [English translation of 1st edn. (Jerusalem, 1969)]
- [22] A. M. Mukhamedzhanov and L. D. Blokhintsev, *Eur. Phys. J. A* **58**, 29 (2022)
- [23] A. M. Mukhamedzhanov, B. F. Irgaziev, V. Z. Goldberg *et al.*, *Phys. Rev. C* **81**, 054314 (2010)
- [24] L. D. Blokhintsev, I. Borbely, and E. I. Dolinskii, *Sov. J. Part. Nucl.* **8**, 485 (1977)
- [25] S. A. Rakitiansky, *Jost Functions in Quantum Mechanics* (Springer Nature Switzerland AG, 2022)
- [26] Y. Yamaguchi, *Phys. Rev. C* **95**, 1628 (1954)
- [27] R. B. Wiringa, V. G. J. Stoks, and R. Schiavilla, *Phys. Rev. C* **51**, 38 (1995)
- [28] R. Machleidt, *Phys. Rev. C* **63**, 024001 (2001)
- [29] O. A. Rubtsova, V. N. Pomerantsev, and M. N. Platonova, *Int. J. Mod. Phys. E* **33**, 2441030 (2024)
- [30] R. B. Wiringa, R. Schiavilla, S. Pieper *et al.*, *Phys. Rev. C* **89**, 024305 (2014)